DOI 10.59887/2073-6673.2023.16(4)-4

UDC 551.466.6

© *D. A. Romanenkov*[1]*, *E. V. Sofina*[1,2], *A. E. Rodikova*[1], 2023
© Translation from Russian: *E. S. Kochetkova*, 2023

[1]Shirshov Institute of Oceanology, Russian Academy of Sciences, 36 Nakhimovsky Prosp., Moscow, 117997, Russia
[2]Russian State Hydrometeorological University, 79 Voronezhskaya Str., St. Petersburg, 192007, Russia
*dmromanenkov@yandex.ru

MODELING OF BAROTROPIC TIDE OFF THE SOUTHEASTERN COAST OF THE KAMCHATKA PENINSULA IN VIEW OF THE ACCURACY OF GLOBAL TIDAL MODELS IN THE NORTHWEST PACIFIC OCEAN

Received 05.08.2023, Revised 10.10.2023, Accepted 13.11.2023

Abstract

This study introduces the development and implementation of a regional numerical finite-volume model FESOM–C, specifically designed to accurately compute barotropic tidal dynamics in the Pacific waters adjacent to the southeastern region of the Kamchatka Peninsula. The dynamics of principal harmonics of the semidiurnal M2 and diurnal K1 tidal constituents are replicated, as well as the total tide, which encompasses 12 constituents. The computed results, obtained using a detailed unstructured grid, are interpreted through the Long-wave approach. The FESOM–C regional model revealed the variability of harmonic constants of tide and current characteristics within the shelf and canyon-cut continental slope, due to topographic scattering of tidal waves. The assessment includes the estimation of maximum currents and eddy structures associated with residual tidal circulation on the shelf and continental slope. To investigate the influence of varying open boundary conditions, sensitivity experiments have been conducted using data from two state-of-the-art global tidal models FES2014 and TPXO9. The findings reveal that the regional model's solution exhibits only minimal dependency on this choice, and it aligns well with the limited available tidal data. Interestingly, the global models themselves demonstrate significant disparities in the tidal currents. Furthermore, we assess the accuracy of global tidal model solutions in a broader region encompassing the Sea of Okhotsk, as well as the Pacific waters along the Kuril Islands and the Kamchatka Peninsula. This assessment utilizes a verified database of tidal harmonic constants derived from the Soviet and British tide tables. While the average errors in tidal heights calculations remain minor and closely approximate officially declared values, certain areas within the region exhibit notable discrepancies in the outputs of the global models. These discrepancies are site-specific and vary depending on the particular model and tidal harmonic under consideration. This underscores the need for caution when applying results from global tidal models at the regional scale. Meanwhile, the importance of advancing regional tidal dynamics modeling remains evident.

Keywords: regional modeling, tide, harmonic constants, residual circulation, vorticity, global tide models, FES2014, TPXO9, FESOM–C model, unstructured grid, Sea of Okhotsk, Kuril-Kamchatka region, Avacha Bay

УДК 551.466.6

© *Д. А. Романенков*[1]*, *Е. В. Софьина*[1,2], *А. Е. Родикова*[1], 2023
© Перевод с русского: *Е. С. Кочеткова*, 2023

[1]Институт океанологии им. П.П. Ширшова РАН, 117997, Нахимовский проспект, д. 36, Москва, Россия
[2]Российский государственный гидрометеорологический университет, 192007, Воронежская улица, д. 79, Санкт-Петербург, Россия
*dmromanenkov@yandex.ru

МОДЕЛИРОВАНИЕ БАРОТРОПНОГО ПРИЛИВА У ЮГО-ВОСТОЧНОГО ПОБЕРЕЖЬЯ П-ВА КАМЧАТКА С УЧЕТОМ ТОЧНОСТИ ГЛОБАЛЬНЫХ ПРИЛИВНЫХ МОДЕЛЕЙ В СЕВЕРО-ЗАПАДНОМ РЕГИОНЕ ТИХОГО ОКЕАНА

Статья поступила в редакцию 05.08.2023, после доработки 10.10.2023, принята в печать 13.11.2023

Аннотация

В настоящей работе представлена реализация численной конечно-объемной региональной модели FESOM–C для предвычисления баротропной приливной динамики в тихоокеанских водах, прилегающих к юго-востоку п-ва Камчатка. Динамика воспроизводится для отдельных гармоник полусуточного M2 и суточного K1 диапазона

Ссылка для цитирования: *Романенков Д.А.*, *Софьина Е.В.*, *Родикова А.Е.* Моделирование баротропного прилива у юго-восточного побережья п-ва Камчатка с учетом точности глобальных приливных моделей в северо-западном регионе Тихого океана // Фундаментальная и прикладная гидрофизика. 2023. Т. 16, № 4. С. 45–62. doi:10.59887/2073-6673.2023.16(4)-4
For citation: *Romanenkov D.A.*, *Sofina E.V.*, *Rodikova A.E.* Modeling of Barotropic Tide off the Southeastern Coast of the Kamchatka Peninsula in View of the Accuracy of Global Tidal Models in the Northwest Pacific Ocean. *Fundamental and Applied Hydrophysics*. 2023, 16, 4, 45–62. doi:10.59887/2073-6673.2023.16(4)-4

приливного спектра, а также для суммарного прилива из 12-ти составляющих. Результаты расчетов, полученные на детальной неструктурированной сетке, интерпретируются в рамках волнового подхода. Региональная модель выявила изменчивость гармонических постоянных приливных колебаний уровня и характеристик течений на шельфе и изрезанном каньонами континентальном склоне из-за топографического рассеивания приливных волн. Оценены максимальные течения и вихревые структуры, связанные с остаточной приливной циркуляцией на шельфе и континентальном склоне. Выполнены эксперименты по чувствительности численного решения к заданию условий на открытых границах, взятых из двух современных глобальных приливных моделей FES2014 и TPXO9. Решение в региональной модели слабо зависит от этого выбора и хорошо согласуется с имеющимися немногочисленными данными по приливам. Однако оказалось, что решения самих глобальных моделей значимо отличаются между собой в поле приливных течений. Дополнительно было сделано сравнение точности решений глобальных приливных моделей для региона, включающего Охотское море и тихоокеанские воды вдоль островов Курильской гряды и п-ва Камчатка. Это сравнение было выполнено для верифицированной базы гармонических постоянных приливного уровня из советских и британских таблиц приливов. Хотя в среднем по области ошибки расчета приливного уровня малы и близки к официально заявленным, в отдельных районах региона ошибки глобальных моделей были весьма значимы. Их географическая привязка зависит от конкретной модели и сравниваемой приливной гармоники. Это означает, что к использованию результатов глобальных приливных моделей на региональном масштабе следует относиться с осторожностью, а актуальность развития регионального моделирования приливной динамики сохраняется.

Ключевые слова: региональное моделирование, прилив, гармонические постоянные, остаточная циркуляция, завихренность, глобальные модели приливов, FES2014, TPXO9, модель FESOM–C, неструктурированная сетка, Охотское море, Курило-Камчатский регион, Авачинский залив

1. Introduction

Precise replication of tides is of utmost importance in the modeling of intricate shelf and coastal processes. It is widely acknowledged that the skill of model physics and the precision of tidal motion calculations depend significantly on several key factors: (1) the availability of a digital bathymetry model of sufficient quality; (2) the use of a high-resolution grid to account for pronounced geometric and bathymetric features; (3) the capability to represent three-dimensional effects with a description of boundary layers. In the context of regional models for marine open areas, it is also necessary to have adequate conditions at the open boundaries of the calculation area, and for expediting the model field adaptation phase (spin-up), proper initial conditions are essential.

Satellite altimetric observations have made a substantial contribution to the understanding of global processes on the sea surface, notably by enhancing the accuracy of ocean tide predictions through data assimilation. It was believed that the quality of global tide models on a regional scale, encompassing shallow waters and coastal areas, fell short in predicting sea level and current characteristics with the precision achieved in open ocean predictions. This assertion was based, in part, on the results of comparisons with seven contemporary global ocean tide models at the time of publication [1]. The primary focus of this comparison was directed towards empirical models, which are based on the processing and interpolation of altimetric data, and hydrodynamic assimilation models, which assimilate altimetric and tide gauge observation data. The testing was grounded in the comparison of model solutions with both in-situ and remote measurements of tidal levels.

In recent years, the reliability of altimetric data in coastal regions has notably improved, thanks to the development and application of new algorithms and technical enhancements, a detailed review of which is presented in [2]. Consequently, more “coastal” signals are extracted compared to the classical altimetry processing, without compromising the accuracy of standard open ocean processing and coastal regions. This, in turn, leads to the increased accuracy of many tidal models utilizing altimetry in areas where it was previously lacking. This has allowed for a reduction in the contribution of data from coastal tide gauges during assimilation, or categorizing certain stations as unrepresentative. In recent years, numerous studies have emerged with a focus on reevaluating the accuracy of global models on a regional scale [3–11]. An analysis of these publications reveals that when compared to observational data and reasonable area-averaged error estimates, these global models may exhibit disparities in certain regions. Furthermore, the results of such comparisons are contingent on the specific tidal harmonic under consideration. For instance, in [12], it is noted that the tidal atlas FES2014 notably enhances accuracy compared to the earlier version, FES2012, with a significant improvement observed in the Arctic Ocean for the tidal constituents K1 and S2. However, a reduction in accuracy appears to have occurred in two anomalous regions: the Ross Sea for O1 and the Weddell Sea for M2.

On the other hand, the accumulated time series of altimetric observations over three decades allow for the assessment of a greater number of minor tidal constituents. As ocean tide models continue to improve, particularly in coastal areas, these minor tides are gaining increasing significance. Currently, the most common global tidal models are TPXO [13] and FES [14]. Based on their latest versions (TPXO9 and FES2014, respectively), tidal harmonic constant atlases are frequently utilized to determine and provide boundary information in regional models. These datasets offer the finest spatial resolution, the most extensive harmonic set, and a low mean calculation error when compared with benchmark coastal and pelagic tide gauges. Although these models have also been among those evaluated in the previously cited studies, to date, there have been no such assessments for the waters of the northwestern Pacific Ocean, including the Sea of Okhotsk and the Kuril-Kamchatka region.

One of the objectives of this study was to conduct regional modeling of barotropic tides in the waters adjoining the southeastern coast of Kamchatka. This modeling will be employed in the following numerical simulations of the complex dynamics and hydrology of this region, characterized by a limited array of heterogeneous observations. Another goal of this study is the assessment of the quality of global models in the overall region, assuming that the proposed regional model, equipped with improved boundary conditions, will provide new insights into the tidal dynamics within these waters.

The paper is structured as follows: In Section 2, information about the research area and the state of its tidal dynamics study is presented. Section 3 provides data on the observed harmonic constants of tide, discussing two different solutions for global tides, namely FES2014 and TPXO9. The regional model is briefly introduced in focus on the discretization characteristics of the computational domain using an unstructured grid. In Section 4, a comparison of global models in the northwestern part of the Pacific Ocean, including the Sea of Okhotsk and the Kuril-Kamchatka region, is conducted among themselves and with observational data. The results of regional modeling are presented in Section 5. The selection of boundary conditions for the regional model is discussed. A general description of the modeled tide is provided for the diurnal (K1) and semidiurnal (M2) harmonics as representatives of sub-inertial and super-inertial tidal forcing harmonics. A separate discussion is dedicated to tidal currents and their distinctions from global model solutions within the study area. The results of modeling the total tide are limited to the analysis of maximum currents, eddy structures, and residual tidal circulation. The Conclusion section addresses the outcomes of the work and the implications derived from them.

2. Research Region

The Pacific Ocean waters adjacent to the southeastern coast of the Kamchatka Peninsula encompass both narrow and wide shelf areas, a steep continental slope, and a deep-sea trench (see Figure 1). The underwater topography of two major bays within this region, Kronotsky and Avacha, is characterized by intricate deep-sea canyons that extend across the slope and the narrow shelf. This area, primarily due to its canyons, is renowned as the spawning ground for the largest population of the Eastern Kamchatka walleye Pollock (Gadus chalcogrammus Pallas) in the region. Our interest in this aquatic region is prompted by existing evidence of potential critical influences of some abiotical processes on the early stages of development of this commercially important fish species, attributed to tidal dynamics [15]. To implement a regional model of the dynamics and hydrology of this area, accounting for tidal impacts, the initial step requires the creation and verification of the tidal component of this model, with particular attention to the specified conditions along the extensive open boundary of the domain. Tidal phenomena within this aquatic region have not been the subject of targeted investigation. As stated in the Introduction, researchers have access to the results of global tide models such as TPXO9 (version 4) and FES2014, which can be employed for initiating the boundary and initial conditions of the regional tidal model. However, the quality of global model solutions in the northwestern Pacific Ocean region has not been thoroughly examined. For the southeastern part of the Kamchatka Peninsula, only two tide gauge stations with harmonic constants of tides are available in open databases, one of which (see Figure 1) is situated in the Avacha Bay and may not be representative for comparison with global model results. Therefore, in the preliminary stages of this study, it was decided to evaluate the quality of global models in a broader region, encompassing the Sea of Okhotsk, the Pacific waters of the Kuril-Kamchatka region, and the northern part of the Sea of Japan.

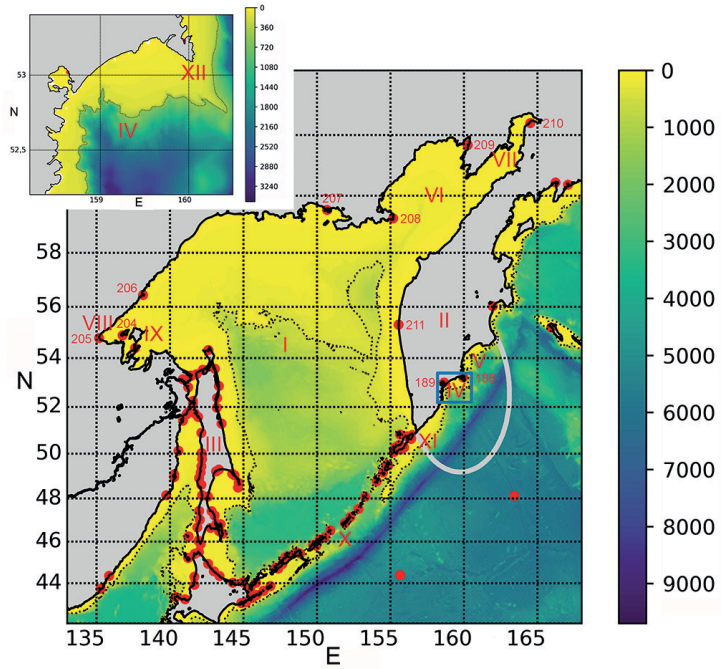

Fig. 1. Bathymetry of the study area (m). Red circles represent observation points with harmonic constants of tidal level amplitudes and phases. Dashed lines indicate the 500 m isobath. The gray curve represents the boundary of the computational domain of the regional model. The blue rectangle denotes the area of the incut with bathymetry near the deep-water canyons of the Avacha Bay. Arabic numerals indicate the mentioned observation points in the text, while Roman numerals mark: I — Sea of Okhotsk, II — Kamchatka Peninsula, III — Sakhalin Island, IV — Avacha Bay, V — Kronotsky Bay, VI — Shelikhov Gulf, VII — Penzhina Bay, VIII — Uda Bay, IX — Shantar Islands, X — Kuril Islands, XI — Lopatka Cape, XII — Shipunsky Cape

The northwestern part of the Pacific Ocean is strongly influenced by tidal dynamics affecting the hydrology of its waters. Notable characteristics of tides in the region include: 1) the dominance of diurnal constituents in the spectrum of mixed type tide in most of its parts, and 2) some of the highest tidal amplitude values in the world, observed in Penzhin Bay and bays of the Shantar region in the Sea of Okhotsk.

The structure of tides and various aspects of their dynamics in the Sea of Okhotsk and the adjacent waters of the Pacific Ocean have been the subject of previous modeling studies [16–26]. Only in [25–26], tidal forcing was applied from TPXO9, and the quality of global models was not assessed in those or other studies. In this context, we do not analyze the results of tidal dynamics modeling in the region, but we will highlight one particular feature. The dynamics of long-wave processes in the region, including tides, are characterized by the generation and propagation of trapped shelf waves (a type of Rossby topographic waves) [27]. Under certain conditions, these waves “extract” energy from the primary barotropic tide of sub-inertial harmonics as it dissipates over bathymetric and shoreline irregularities. Their wavelengths are more than an order of magnitude shorter than the wavelength of the fundamental energy-carrying Kelvin wave, which manifests in observed small-scale variations in the characteristics of sea level oscillations and currents [28]. This circumstance may prove challenging for both modeling and the comparison of its results with observational data.

3. Initial Data and Research Methodology

3.1 Database of Harmonic Constants of Tide

Existing open tidal observation data include harmonic constants tables for tidal levels from 1948 and 1960 [29–30] and Admiralty tidal tables from 1998 [31]. The primary data source consisted of Soviet tables (118 stations), and the dataset was augmented with Admiralty tables (95 stations), including 4 unique stations not present in the Soviet tables, along with 2 pelagic stations [32]. In the initial stage, data verification was conducted through cross-comparisons between different datasets, comparisons with known tidal charts, and the WXTIDE32 tidal calculator database [33]. As a result, station coordinates and certain amplitude and phase values of tide were adjusted, and the phase was converted to UTC time. Errors and typos were identified in both datasets. Dubious stations were excluded, and duplicates were not considered. This phase yielded a new base of harmonic constants containing 124 tidal stations (supplementary materials: Appendix, Table A1).

3.2 Global tidal models

Below, a more detailed examination of the most common databases concerning the characteristics of tidal harmonics, TPXO, and FES, obtained using global models with data assimilation, will be provided.

TPXO (Oregon State University TOPEX/Poseidon Global Inverse Solution tidal model) is a global product based on a barotropic tidal model that assimilates altimetry data from satellites such as Topex Poseidon, Topex Tandem, ERS, GFO, and in situ observations from tidal gauges. Each successive version of the TPXO model is based on updated bathymetry and assimilates more data compared to its predecessors. The latest available implementation, TPXO9, features a spatial resolution of 1/30°.

The model description and assimilation procedure are presented in [13]. The archive comprises harmonic constants (amplitudes and phases of tide) and constituents (northward and eastward components) of barotropic (vertically-averaged) tidal currents. It also includes local bathymetry used to calculate tidal flows (velocity components multiplied by local depth) for tidal constituents, such as M2, S2, N2, K2, K1, O1, P1, Q1, the long-period components Mf and Mm, and the nonlinear constituents M4, MS4, MN4, as well as 2N2 and S1.

The FES2014 (Finite Element Solution) global ocean tide atlas is a global product created based on a finite element barotropic tidal model with spatial resolution ranging from 2 to 60 km depending on local depth. The atlas is the result of assimilating long time series of altimetric data from satellites such as Topex/Poseidon, Jason-1, Jason-2, TP interleaved-J1 interleaved, ERS-1, ERS-2, and Envisat, along with in situ observational data from tidal gauges. The model description and assimilation procedure are provided in [14].

The FES2014 atlas includes harmonic constants (amplitudes and phases of tide and components of barotropic tidal currents in the north and east directions) and loading tide (vertical displacements of the Earth's crust due to oceanic tides) for the following tidal harmonics: 2N2, EPS2, J1, K1, K2, L2, La2, M2, M3, M4, M6, M8, Mf, MKS2, Mm, MN4, MS4, MSf, MSqm, Mtm, Mu2, N2, N4, Nu2, O1, P1, Q1, R2, S1, S2, S4, Sa, Ssa, and T2. The user-accessible database is provided on a regular grid with a spatial resolution of 1/16°, obtained through interpolation from the "native" finite element grid. Additionally, there is an extrapolated version of the database available for tidal levels, though not for current velocities, to cover coastal regions more comprehensively.

3.3 Regional model FESOM–C

3.3.1 Description of the Regional Model

To simulate the barotropic tides in the Pacific waters southeast of the Kamchatka Peninsula, the Finite Element Sea-ice Ocean Model, FESOM–C (FESOM–Coastal, [34]), was employed. This model forms the basis for addressing a wide range of geophysical, hydrogeological, engineering, and environmental problems. FESOM–C is founded on the discretization of the original geophysical hydrodynamics equations using the finite volume method and operates on horizontal mixed unstructured grids composed of triangles and quadrilaterals. FESOM–C possesses multi-resolution functionality for simulating marine hydrodynamics, bridging the gap between different motion scales. The model employs multiple advection schemes for the equations of motion and tracers, characterized by low numerical dissipation. It is equipped with modules for tide, drying, and sedimentation calculations. For the vertical coordinate, a standard sigma-coordinate transformation is used, which accounts for bathymetry. The numerical implementation of the model in the horizontal direction is based on an explicit scheme that separates the barotropic (mean in the vertical) and baroclinic modes. The model features two types of parallelization: Open MPI and MPI. The dynamic core of FESOM–C has been developed and tested (in the hydrostatic option) in numerous idealized and real-world experiments [34–38]. The 2019 version of the FESOM–C model is accessible at the following link: https://doi.org/10.5281/zenodo.2085177 (accessed on June 27, 2023).

In this study, the FESOM–C model is utilized to compute the barotropic tides (without accounting for stratification effects). Thanks to the model's adopted algorithm, which splits the dynamic problem into the vertical mean and deviations from it, model solutions in three-dimensional and two-dimensional (shallow water approximation) formulations for variables such as sea level and vertical mean velocities are nearly indistinguishable. In our analysis, we will focus on precisely these variables and the associated dynamical characteristics. The Smagorinsky model is employed to describe horizontal eddy viscosity. To approximate advection, a second-order accurate finite difference scheme is selected. The bottom friction coefficient is set to 0.005. To stabilize the numerical solution near the open boundary and reduce the time for solution convergence, an additional buffer zone option is used along this boundary, with a width of 20 km and a bottom friction coefficient increased by a factor of 10.

3.3.2. Grid

The calculations were conducted on an unstructured triangular mesh with elements of uniformly varying sizes. The mesh was generated using the GMSH generator [39], with local refinement allowing for a reliable representation of the barotropic scale $\left(L_{bt} = \sqrt{gh}\right) \Big/ \left(\max\left(f, \omega\right)\right)$ according to the recommendations [40], where $g = 9.81$ m/s², h represents the local depth, f is the Coriolis parameter, and ω is the tidal harmonic frequency. In our model domain $L_{bt} \in$ [50 km to 2500 km], with a total of 37,738 nodes in the mesh and 74,226 elements. The edge sizes of the elements range from 330 m to 7800 m, with the smallest values in the shallow water areas.

The bathymetry of the computational domain was derived from the 30″ ETOPO 2022 dataset [41], with minimum and maximum depths of 5 m and 7900 m, respectively. This version of the archive effectively resolves deep canyons in the bays (Fig. 1, inset).

3.3.3. Boundary Conditions

At the open boundary of the model domain, the sea level is set in the form of:

$$\xi = \xi_0 + \sum_{i=1}^{n} f_i A_i \cos(\omega_i t + (\upsilon_0 + u_i)_i - g_i), \quad (1)$$

where n represents the number of considered harmonics (waves), ξ_0 is the non-tidal component of sea level variations, A_i denotes the amplitude of tidal wave i, $\omega_i = 2\pi/T_i$ represents the angular velocity of wave i (in radians per second), T_i is the period of the i-th harmonic, t is the time, g_i is the phase of wave i relative to the prime meridian, determining its initial sea level reference at the initial time of the calculation $t = 0$, f_i represents the astronomical nodal factor, and $(v_0+u)_i$ signifies the astronomical argument. A_i and g_i are the tidal harmonic constants, which depend on local conditions and are provided from observations or other models. The values of f_i and $(v_0+u)_i$, the astronomical parameters at "00" hours of the first day of the calculation, are determined based on the lunar and solar orbit parameters in accordance with [42].

To calculate the monoperiodic tide, one of two harmonics is specified: the semi-diurnal M2 (T = 12.42 hours) or the diurnal K1 (T = 23.93 hours), without considering astronomical parameters. For the total tide, the following constituents are considered: M2, S2, N2, K2, K1, O1, P1, Q1, Mf, Mm, MS4, M4. Other calculation parameters include $\xi_0 = 0.0$, a time step of $\Delta t = 3$ seconds. The calculations are performed until the numerical solution reaches a quasi-periodic regime, where the mean change in the depth-integrated barotropic tidal energy density becomes less than 0.1 % over a tidal cycle and the entire sea area. The monoperiodic tide stabilizes in less than 20 periods, and the total tide takes approximately 4 synodic months to establish. To estimate the harmonic constants of the monoperiodic tide, a Fourier analysis was conducted on the numerical solution over the last tidal cycle of the calculation. The analysis of the total tide was performed for one synodic month after the solution had stabilized.

4. Comparison of global models among themselves and with observational data

The analysis of tidal maps for the diurnal (K1, O1) and semidiurnal (M2, S2) harmonics in the northwestern region of the Pacific Ocean revealed that large-scale tidal features, such as the number and positions of amphidromes, local maxima, and minima, correspond to established understanding of tides in the region (see, for example, [18, 43]). However, there are differences in the values of tidal characteristics.

Comparison of the results from the global models FES2014 and TPXO9 was conducted for the observation points included in the newly corrected database of harmonic constants of tidal level amplitudes and phases (see Table A1; Figure 1).

Spatial maps of the vector error of tidal heights from global models for the harmonics M2, S2, K1, and O1 are presented in Fig. 2. The vector error was determined as follows:

$$D_i = \left\{ \frac{1}{T} \int_0^T \left[A_{oi} \cos\left(\omega t - g_{oi}\right) - A_{mi} \cos\left(\omega t - g_{mi}\right) \right]^2 dt \right\}^{1/2} = 2^{-1/2} \left[A_{oi}^2 + A_{mi}^2 - 2 A_{oi} A_{mi} \cos\left(g_{oi} - g_{mi}\right) \right]^{1/2}, \quad (2)$$

where A_{oi}, g_{oi}, A_{mi}, and g_{mi} are the observed and model values of amplitude and phase of tide at the i-th observation point for an individual tidal harmonic with period T.

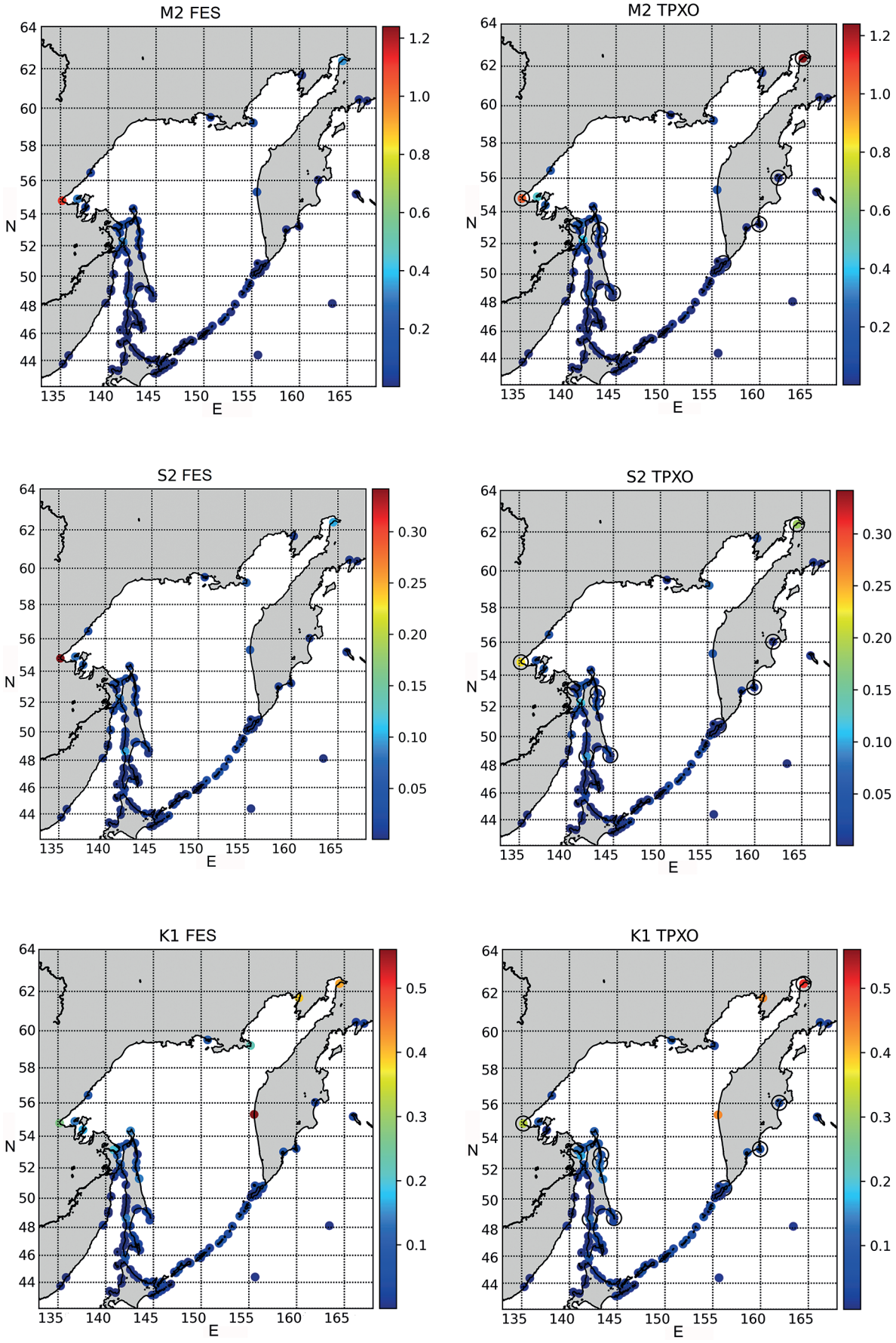

Fig. 2. Fin p. 52

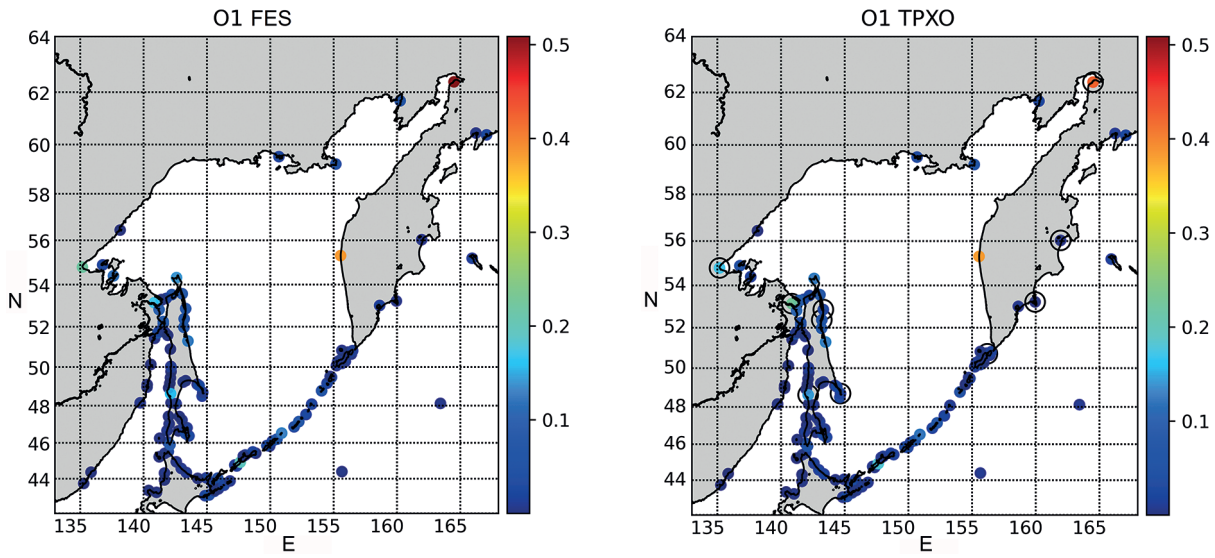

Fig. 2. Vector errors in tidal heights (m) using global models FES2014 and TPXO9 at observation points (supplementary materials: Appendix, Table A1) for the M2, S2, K1, and O1 tidal constituents. Error magnitude is indicated by color, with black circles denoting points where coordinates did not fall within the model grid cell, and harmonic constants were assumed equal to the constants at the nearest grid node

In most locations, the vector error does not exceed a few centimeters for all four harmonics. Exceptions are Cape Astronomical and Uda Bay (stations 210 and 205 respectively), where the tides are the highest in the region (see Table A1). The error magnitude might also be affected by the station locations; both stations are at the bay heads. For example, at Lebyazhya Bay on the Shantar Islands (station 204), located to the east of station 205, the vector error is small, despite the significant tidal amplitudes. Significant discrepancies are observed at station 211, located at the mouth of a river on the western coast of Kamchatka, for both diurnal harmonics, and in station 209 in the northwestern part of Shelikhov Bay for the K1 harmonic. The latter example errors may be generated by both model and inaccuracies in the observational data. It is worth noting a slight increase in vector errors on the northeastern coast of Sakhalin for diurnal harmonics, which could be attributed to the influence of shelf waves in this area [44].

In Fig. 3, probability distributions of vector errors are presented for the four harmonics and both global models. A lower median value compared to the mean is characteristic for all vector errors, indicating the presence of individual large outliers. Based on the mean values of vector errors, FES2014 appears more favorable compared to TPXO9, while the error medians are close, and Q3 (the third quartile) for TPXO9 is smaller, as well as the "whiskers." This conclusion does not apply to S2, where error distributions for both global models are nearly identical. The significantly high mean values of vector errors in TPXO9 for the M2 and K1 harmonics are due to the outliers in the aforementioned two locations: Cape Astronomical (station 210) and Uda Bay (station 205). Bilinear interpolation was used for the interpolation of modeling results for both models. When the coordinates of the stations did not fall within the computational grid cell, the harmonic constants for those points were set equal to the values at the nearest grid node. The coordinates of both stations extend beyond the TPXO9 computational domain (in Fig. 2, these points are encircled in black). For the FES2014 model, all harmonic constants were obtained through bilinear interpolation, as an extrapolated archive of FES2014 model results was used.

Upon a more detailed examination of station 210, Cape Astronomical (refer to Table A1), it becomes evident that the discrepancy in the M2 amplitude between observational data and the TPXO9 model is significantly smaller than that observed in the FES2014 model. To be specific, it measures 0.085 meters in contrast to –0.322 meters. Additionally, the vector error stands at 0.34 meters for FES2014 and 1.24 meters for TPXO. This disparity is primarily attributed to a notable phase shift in the Penzhinskaya Gulf apex within the TPXO9

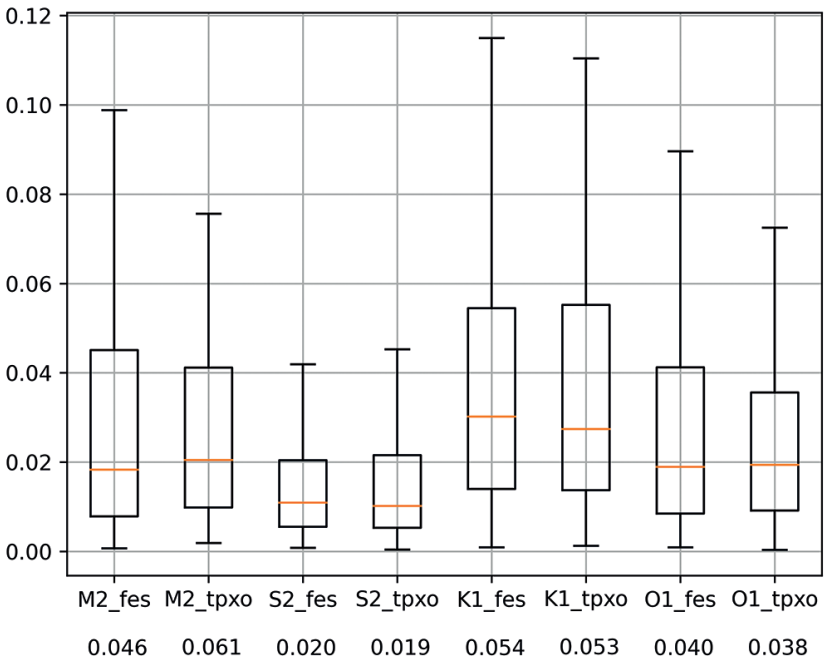

Fig. 3. Probability diagram of vector errors (box plot). The box boundaries correspond to Q1 and Q3 (first and third quartiles), the orange line represents Q2 (the median), and the whiskers extend to 1.5 × (Q3 — Q1) from the edges of the box, ending at the farthest data point within this interval. Outliers are not depicted. The lower row provides the mean values of vector errors (m)

model, recording a phase of 340° compared to the observed 261°. This difference may be explained by the bathymetry data for this region, representing greater depths than the actual bathymetry. Another plausible explanation lies in the implementation of an unstructured grid in the FES2014 model simulation, which facilitates a more detailed depiction of the coastline and increased resolution within narrow bays. These differences in sea level characteristics are expected to be reflected in the patterns of tidal currents. In order to compare these

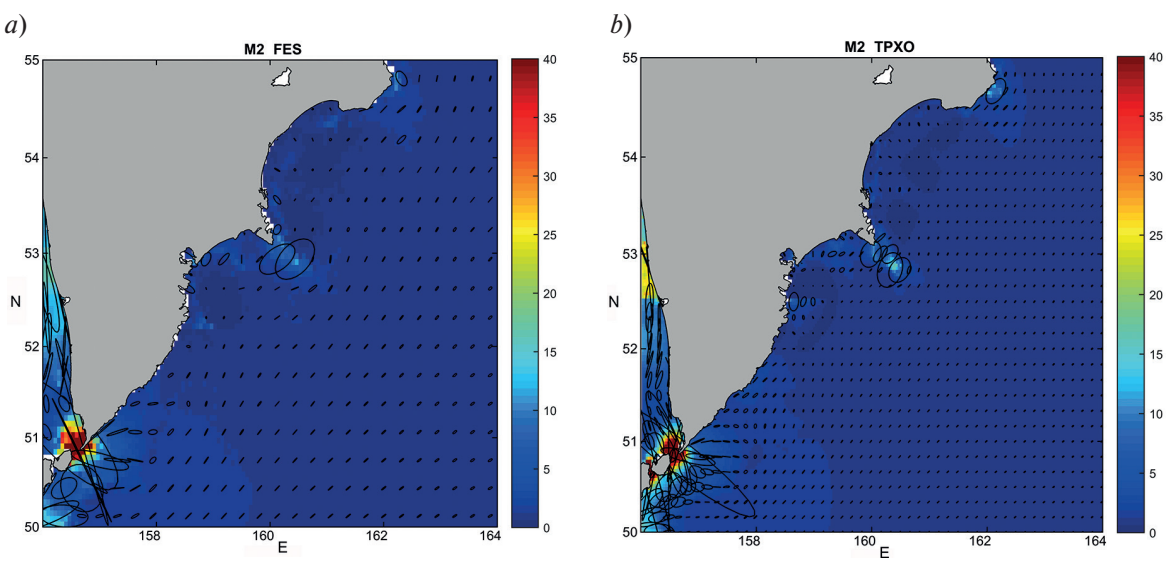

Fig. 4.Fin p. 54

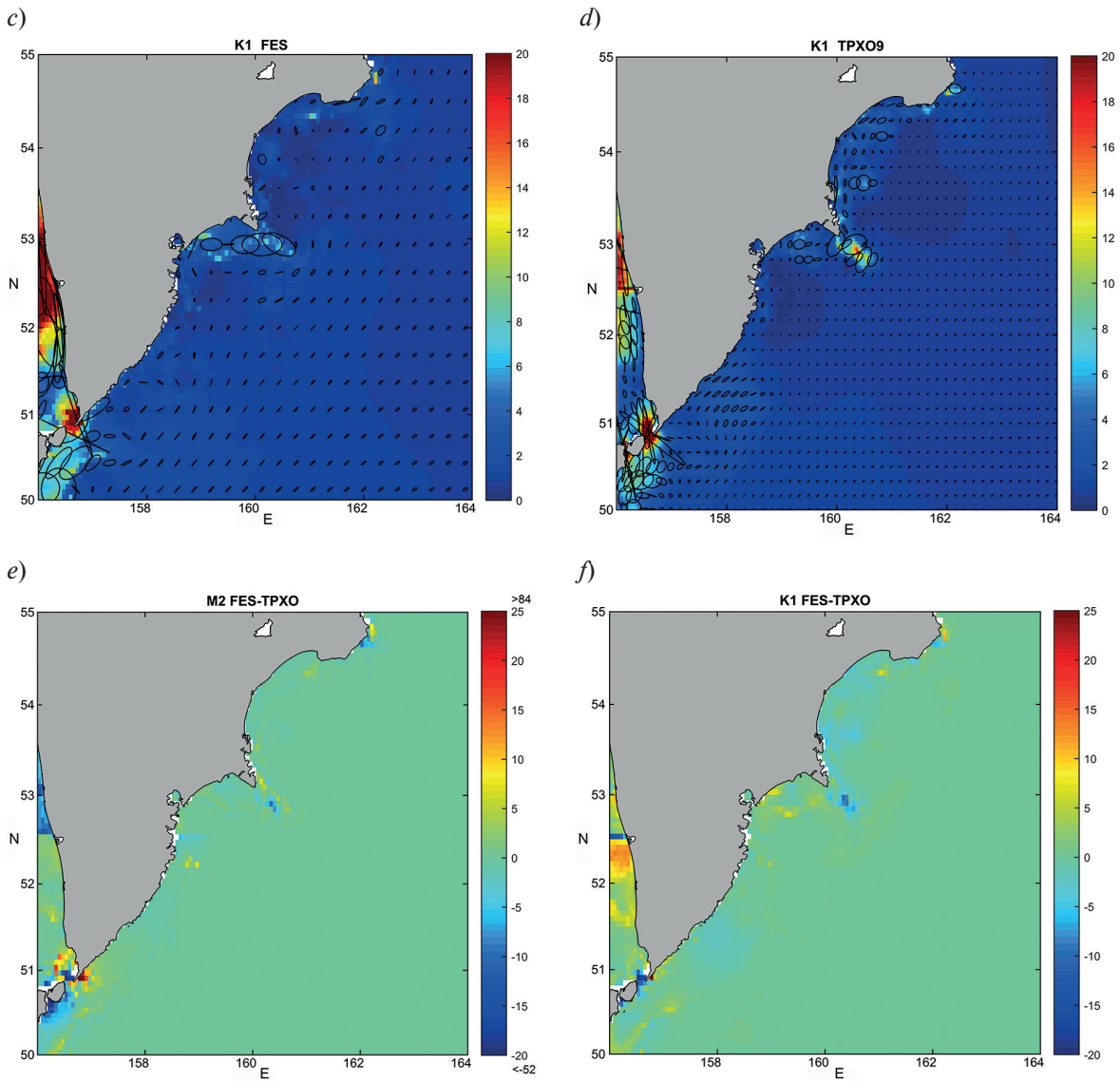

Fig. 4. Tidal current ellipses and amplitude of tidal current velocities (major axis of tidal ellipse) in global models for harmonics M2 and K1: *a* — M2 currents from FES2014; *b* — M2 currents from TPXO9; *c* — K1 currents from FES2014; *d* — K1 currents from TPXO9; *e* — difference in the magnitude of the major axis of M2 between FES2014 and TPXO9; *f* — difference in the magnitude of the major axis of K1 between FES2014 and TPXO9. The amplitudes of tidal current velocities are depicted in color, and the ellipses are displayed at every 5 grid nodes. The difference in current velocities is presented at a coarser resolution for the FES2014 model. Current velocities are given in cm/s

currents derived from the global models, we narrow our focus to a region of particular interest: the waters adjacent to the southeastern coast of the Kamchatka Peninsula. Tidal currents are typically represented as ellipses describing the rotation of the current vector over a tidal period for individual harmonics. The ellipse is characterized by its parameters: major and minor axes and the aspect ratio (eccentricity), whose sign indicates the direction of rotation. Figure 4 illustrates the tidal harmonic ellipses from the global models and the disparities in model current amplitudes (major axes of the ellipses). These figures reveal significant disparities in the results, which can reach half or more of the maximum current values. This is particularly evident in the vicinity of the First Kuril Strait. Along the Kamchatka Shelf and the continental slope, these differences manifest locally, primarily in areas characterized by distinct bathymetry and coastlines. Nevertheless, these disparities can be as substantial as ±20 cm/s.

5. Results of Regional Modeling in the Waters Adjacent to the Southeast of the Kamchatka Peninsula

5.1 Comparison of Regional and Global Modeling Results. Sensitivity to the Boundary Conditions

The Table presents the modeling quality assessments for diurnal and semidiurnal harmonics at two observation points in the model domain along the southeast coast of Kamchatka. The table includes differences in amplitude and phase calculations, as well as vector errors compared to similar assessments provided by global models for these stations. It is evident that, for the majority of the compared characteristics, our solution exhibits lower accuracy compared to the FES2014 atlas but performs better than the TPXO9 data. Importantly, our solution does not employ any assimilation procedures. The differences are relatively minor and reflect local peculiarities of oscillations within the bays. Consequently, the regional model's accuracy demonstrates the successful simulation of barotropic tides along the southeast coast of Kamchatka.

Regarding the sensitivity of the regional model to the boundary conditions, the comparison of modeling results has shown that tidal sea level variations are weakly sensitive to the choice between the global models FES2014 and TPXO9 as sources of information on tidal sea level variations at the open boundary. If the choice is based on a comparison at two observation stations, the use of the FES2014 model results in a reduction of the vector error by no more than 0.6 cm for K1, and for M2, the results are nearly identical.

Next, the results of regional modeling are analyzed, where tidal sea level variations at the open boundary are specified from the global model TPXO9. This choice was made because the TPXO9 model provides results with higher resolution, which are more suitable for the end user and are more commonly used by other users.

Table

Model errors of harmonic constants at observation stations. Errors of FESOM–C model are presented with boundary conditions from FES2014 and TPXO9

Station	Source	Harmonic	Amplitude, m	Phase, degrees	Amplitude difference, m	Phase difference, degrees	Vector error, m
St. 188 «Bukhta Morzhovaya», 53.23°N, 159.95°W	observations	M2	0.280	131.0			
	fesom_fes2014		0.268	123.2	0.012	7.8	0.028
	fesom_tpxo9		0.269	122.9	0.011	8.1	0.028
	fes2014		0.279	125.9	0.001	5.1	0.018
	tpxo9		0.282	125.5	–0.002	5.5	0.019
	observations	K1	0.390	334.0			
	fesom_fes2014		0.382	345.5	0.008	–11.5	0.055
	fesom_tpxo9		0.371	346.8	0.019	–12.8	0.061
	fes2014		0.377	344.7	0.013	–10.7	0.051
	tpxo9		0.365	349.4	0.025	–15.4	0.074
St. 189 "Petropavlosk» 53.02°N, 158.63°W	observations	M2	0.320	136.0			
	fesom_fes2014		0.300	129.4	0.020	6.6	0.029
	fesom_tpxo9		0.303	129.4	0.017	6.6	0.028
	fes2014		0.284	132.6	0.036	3.4	0.028
	tpxo9		0.300	131.4	0.020	4.6	0.022
	observations	K1	0.430	333.0			
	fesom_fes2014		0.387	349.2	0.043	–16.2	0.087
	fesom_tpxo9		0.379	350.1	0.051	–17.1	0.092
	fes2014		0.384	348.1	0.046	–15.1	0.082
	tpxo9 *		0.371	351.3	0.059	–18.3	0.099

Note: * The station's location extends beyond the source data area; the «nearest neighbor» extrapolation method was applied.

5.2 Tidal maps

The tidal maps of the major semi-diurnal (M2) and diurnal (K1) harmonics do not exhibit fundamental differences in the spatial patterns of amplitudes and phases (Fig. 5). Phases increase in the southwest direction, and amplitudes gradually rise from the deep-sea areas towards the coast. Such a tidal chart is typical for the large-scale Kelvin tidal wave. The Kelvin wave propagates along the continental shelf, where variations in depth and the coastline introduce some variability in the characteristics of sea level fluctuations. Local amplitude maxima are observed at Cape Shipunsky and in the Avacha Bay, and they are more pronounced for the diurnal K1 harmonic. It is also notable that along the continental slope and on the shelf, amplitudes and phases of the K1 harmonic exhibit more variability compared to the semi-diurnal M2 harmonic. In the vicinity of Cape Lopatka, the peculiarities of the model solution are associated with the gradient of prescribed sea level characteristics at the open boundary, influenced by the nearby First Kuril Strait.

5.3 Monoperiodic tidal currents

Figure 6 represents the tidal currents of the M2 and K1 harmonics. diurnal tidal currents dominate over the semidiurnal currents, exhibiting an intensification not only over the shoal near Cape Shipunsky but also on the shelf in the northern part of the Avacha Bay and in the southwestern region where the shelf widens noticeably. This phenomenon may be associated with the generation of diurnal shelf waves, the effects of which are manifested stronger in the variability of currents. Over shallow shelf areas, both components of the currents deviate from a nearly-reverse regime, and the compression of ellipses decreases, which is typical in zones with high energy dissipation by bottom friction. The spatial structure of the currents is similar to what was previously examined for solutions from global models. Our velocity amplitude solution is closer to the FES2014 current field, except in the southwestern part of the model domain, under the condition that boundary information was adopted from the TPXO9 model.

5.4 Total tide

In the model calculations, the total tide is set at the boundary as a combination of 12 harmonic constituents and computed from January 1, 2022. For analysis, the results of modeling over a synodic month of 29.5 days, corresponding to June 2022, were selected. This month was chosen as a period in which the maximum tidal values are observed according to astronomical conditions from 2016 to 2023.

In Figure 7, the characteristics of the total tidal currents are presented. Maximum current velocities can reach up to 40 cm/s south of Cape Shipunsky. Elevated velocity values are observed in the Avacha Bay, includ-

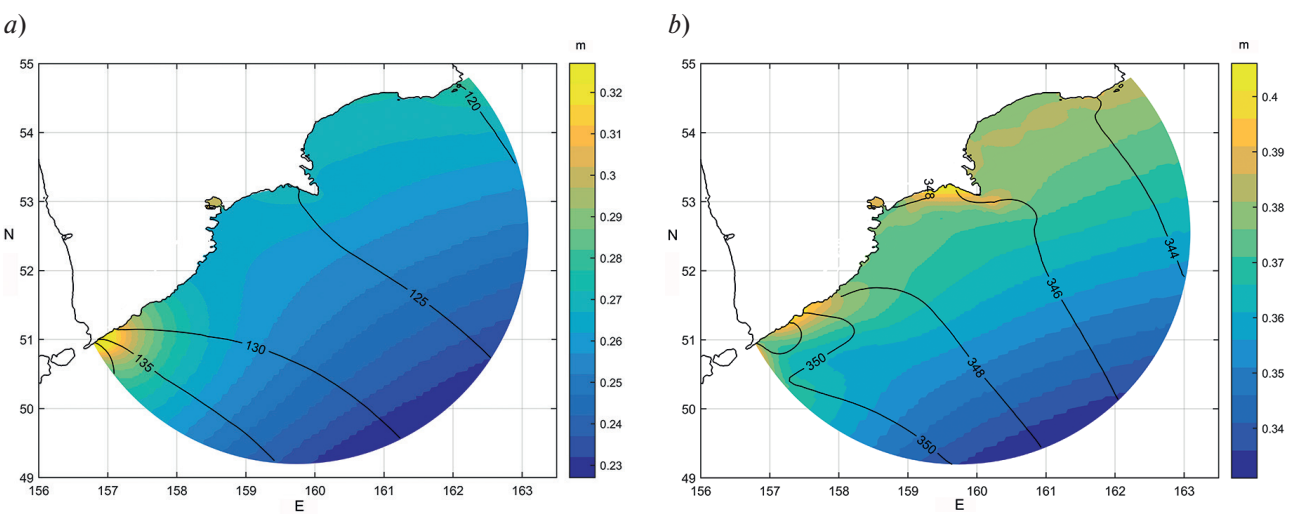

Fig. 5. Tidal maps for principal harmonics (regional model): *a* — M2; *b* — K1. The amplitude is shown using a color scale. Solid lines (cotidal lines) represent phase values in degrees, referenced to the zero meridian

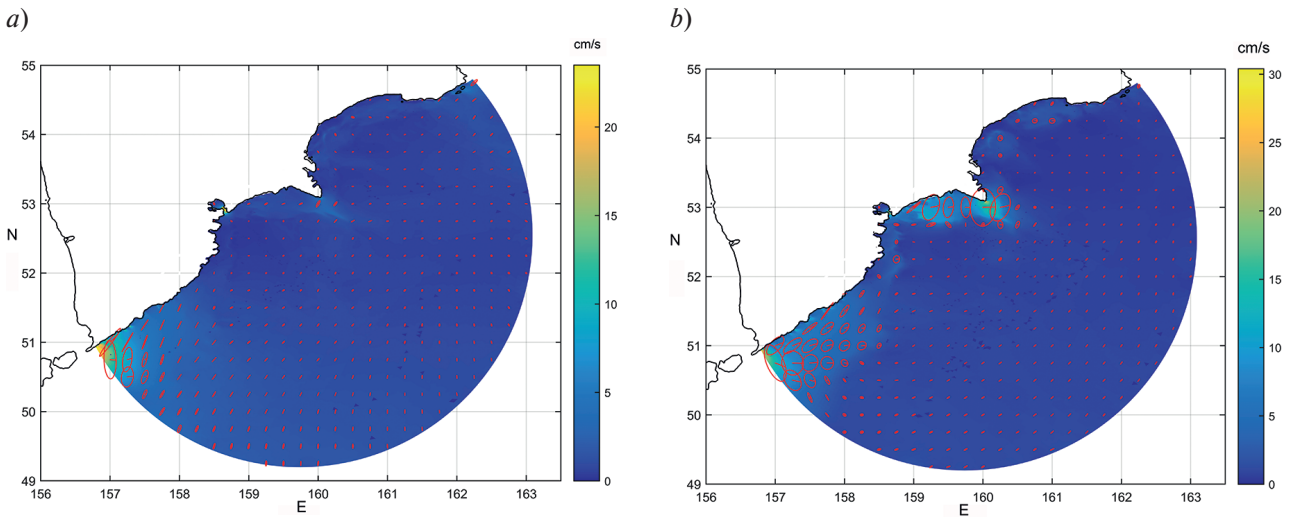

Fig. 6. Tidal current ellipses of principal harmonics (regional model): *a* — M2; *b* — K1. The amplitude of tidal current velocity (major axis of tidal ellipse) is represented by color. The ellipses are shown after interpolating current characteristics onto a uniform grid

ing over deep canyons, and further along the entire southeast Kamchatka shelf. In Kronotsky Bay, the currents are noticeably weaker. Of particular interest is the residual tidal circulation, obtained by averaging the current velocities and relative vorticity over the analysis period, $\zeta = \frac{\partial v}{\partial x} - \frac{\partial u}{\partial y}$, where *u* and *v* represent the zonal and meridional components of the velocity in the right-handed coordinate system, with the x-axis pointing east, the y-axis north. Residual currents result from the nonlinear interaction of the flow with sharp topography and between individual tidal harmonics. This type of circulation plays a crucial role in the dynamics of the continental shelf, ensuring steady transport, causing upwelling, and forming long-lived vortex and convergence zones in the currents. As shown in Fig. 7, *b*, the tide creates a background southwestward transport throughout the region and an anticyclonic eddy south of Cape Shipunsky. Local extremes in the field of residual tidal vorticity (Fig. 7, *a*, inset) indicate that vortex structures on the shelf and slopes of the bays are ubiquitous. Along the canyon slopes, the model predicts sheared residual tidal currents, which are evident from sharp vorticity gradients with a change in sign.

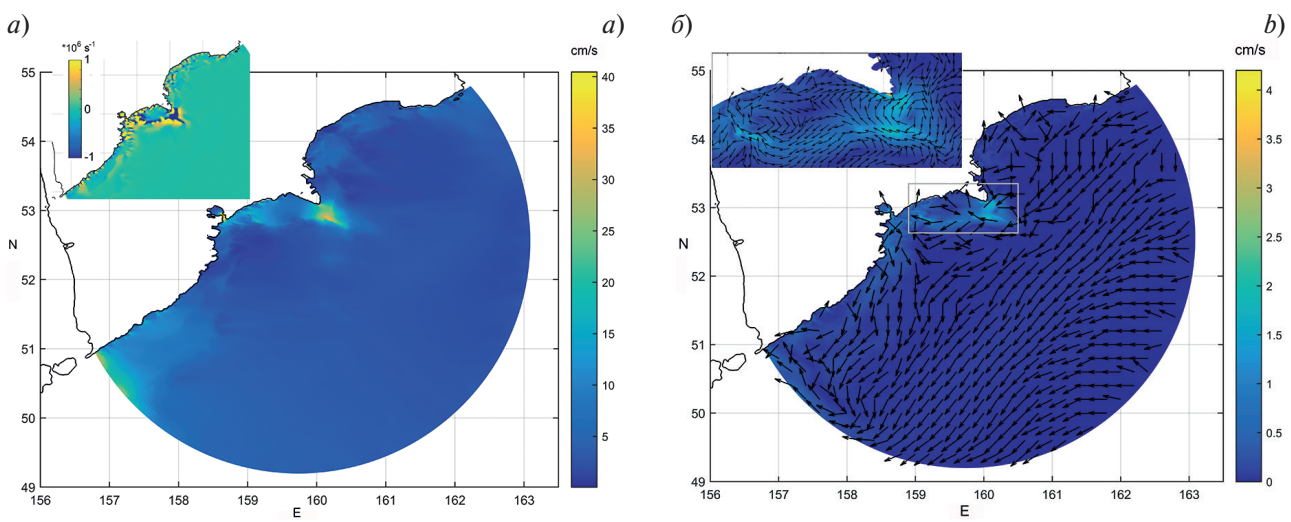

Fig. 7. Results of modeling the total tidal currents: *a* — maximum currents for the synodic month; *b* — residual (average) currents for the synodic month, interpolated onto a uniform grid. Insets in a and b show the residual vorticity and circulation, respectively

6. Conclusions

The numerical model of tidal dynamics has been successfully implemented to simulate barotropic tides along the southeastern part of the Kamchatka Peninsula and the adjacent waters. New detailed tidal level and current maps of the main tidal harmonics in the area have been obtained. The characteristics of the modeled tide are explained from the perspective of wave physics: the tidal structure is dominated by Kelvin waves, and the diurnal harmonic significantly reflects the influence of trapped shelf waves, which manifest in the alongshore variability of tidal characteristics, although less pronounced for the semidiurnal component. Modeling of the total tide has been performed for the first time in this region. Maximum currents and vortex structures associated with tidal currents have been estimated. The calculations have revealed significant residual tidal dynamics on the shelf and continental slope of the Avacha Bay.

The tidal modeling was preceded by a reassessment of the information available from global tidal atlases TPXO9 and FES2014. It has been previously reported that global ocean tide models exhibit significant discrepancies in shallow coastal waters. Our analysis, conducted for the northwestern part of the Pacific Ocean, indicates that these discrepancies may not be limited to these specific areas. None of the global models demonstrates consistently superior performance in certain areas of this region when compared to observational data, especially in the Sea of Okhotsk. These areas can have large tidal level amplitudes, strong tidal currents (e.g., in straits), and unusual local effects generated, for example, by trapped shelf waves. However, the regional average errors (obtained by averaging over all observation points) are low and close to the stated accuracy estimates. Discrepancies with observations can be attributed to both data assimilation methods and the grid resolution used in global tidal models.

Another source of errors is inaccurate coastal observation data. It is unknown which of the tide gauge stations were used for assimilation in global models and which were used for comparisons and accuracy assessments. A review of open reference sources for information on harmonic constants of tides in the northwestern Pacific region was conducted. Errors and typos identified during the analysis of this information were corrected. As a result, a new verified database of tide harmonic constants in the region was used for our assessments of the spatial distribution of errors in global models in the region.

Our results indicate that data obtained from assimilation-based global tidal models should be viewed critically, for instance, in tidal energy assessments or when prescribing boundary conditions in regional modeling. In this case, the choice of boundary conditions from two possible sources had minimal impact on modeling results in the waters adjacent to the southeastern part of the Kamchatka Peninsula. The accuracy of the regional model, without using data assimilation, is comparable to global models when compared with coastal tide gauge stations. Unfortunately, information on tidal current observations is lacking in the area where the tide was modeled. At the same time, significant discrepancies were demonstrated between data from global models in the same area concerning the characteristics of maximum tidal currents, which reach half of their velocity magnitude. Calculated diurnal and semi-diurnal tidal currents from the regional model are close to global solutions in some parts of the region, while they differ in others. These contradictions motivate further research.

Supplementary materials

Appendix. https://www.doi.org/10.59887/2073-6673.2023.16(4)-4-suppl

Acknowledgements

Gratitude is extended to A.A. Androsov for consultations regarding the FESOM–C model and to V.A. Proshchakova for assistance with digitizing tide tables.

Funding

This work was supported by the Russian Science Foundation, project No. 23-17-00174, https://rscf.ru/en/project/23-17-00174/.

References

1. *Stammer D.*, *Ray R.D.*, *Andersen O.B.* et al. Accuracy assessment of global barotropic ocean tide models. *Reviews of Geophysics.* 2014, 52, 243–282. doi:10.1002/2014RG000450
2. *Cipollini P.*, *Benveniste J.*, *Birol F.* et al. Satellite altimetry in coastal regions. *Satellite altimetry over oceans and land surfaces* / Eds. Stammer D., Cazenave A. CRC Press: Boca Raton, FL, USA, 2017. pp. 343–380. doi:10.1201/9781315151779-11

3. *Ranji Z.*, *Hejazi K.*, *Soltanpour M.*, *Allahyar M.R.* Inter-comparison of recent tide models for the Persian Gulf and Oman Sea. *Coastal Engineering Proceedings*. 2016, 35, currents. 9. doi:10.9753/icce.v35.currents.9
4. *Fu Y.*, *Feng Y.*, *Zhou D.* et al. Accuracy assessment of global ocean tide models in the South China Sea using satellite altimeter and tide gauge data. *Acta Oceanologia Sinica*. 2020, 39, 1–10. doi:10.1007/s13131-020-1685-y
5. *Sun W.*, *Zhou X.*, *Zhou D.*, *Sun Y.* Advances and accuracy assessment of ocean tide models in the Antarctic Ocean. *Frontiers in Earth Science*. 2022, 10. doi:10.3389/feart.2022.757821
6. *Khomsin D.*, *Pratomo G.*, *Rohmawati C.N.* Analysis of accuracy comparison tidal global (FES2014, TPXO9) and regional (BIG Prediction) models to the existing tides in Surabaya and surrounding waters. *IOP Conference Series: Earth and Environmental Science*. 2021, 936, 012028. doi:10.1088/1755-1315/936/1/012028
7. *Hart-Davis M.G.*, *Dettmering D.*, *Sulzbach R.* et al. Regional Evaluation of Minor Tidal Constituents for Improved Estimation of Ocean Tides. *Remote Sensing*. 2021, 13(16), 3310. doi:10.3390/rs13163310
8. *Lee J.-C.*, *Lee D-H.* Accuracy assessment of recent global ocean tide models using tide gauge measurements from the East Sea of Korea. *Journal of Coastal Research*. 2023, 39(2), 354–359. doi:10.2112/JCOASTRES-D-22TM-00010.1
9. *de Azkue M.F.*, *D'Onofrio E.E.*, *Jacobs A.* Assessing the accuracy of ocean tide models by using variance of residuals of satellite sea level heights in the Patagonian shelf. *Anales Del Instituto De La Patagonia*. 2022, 50. doi:10.22352/AIP202250004
10. *Ahn J.E.*, *Ronan A.D.* Impact of discrepancies between global ocean tide models on tidal simulations in the Shinnecock Bay area. *Journal of Waterway, Port, Coastal, and Ocean Engineering*. 2019, 145(2). doi:10.1061/(ASCE)WW.1943-5460.0000500
11. *Saraceno M.*, *D'Onofrio E.E.*, *Fiore M.E.*, *Grismeyer W.H.* Tide model comparison over the Southwestern Atlantic Shelf. *Continental Shelf Research*. 2010, 30(17), 1865–1875. doi:10.1016/j.csr.2010.08.014
12. *Ray R.D.*, *Loomis B.D.*, *Luthcke S.B.*, *Rachlin K.E.* Tests of ocean-tide models by analysis of satellite-to-satellite range measurements: an update. *Geophysical Journal International*. 2019, 217, 1174–1178. doi:10.1093/gji/ggz062
13. *Egbert G.D.*, *Erofeeva S.Y.* Efficient inverse modeling of barotropic ocean tides. *Journal of Atmospheric and Oceanic Technology*. 2002, 19(2), 183–204. doi:10.1175/1520-0426(2002)019<0183: EIMOBO>2.0.CO;2
14. *Lyard F.*, *Allain D.*, *Cancet M.*, *Carrère L.*, *Picot N.* FES2014 global ocean tide atlas: design and performance. *Ocean Science, European Geosciences Union*. 2021, 17, 615–649. doi:10.5194/os-17-615–2021
15. *Varkentin A.I.*, *Saushkina D.Y.* Some issues of walleye pollock reproduction in the pacific waters adjacent to the Kamchatka peninsula and the northern Kuril Islands in 2013–2022. *Trudy VNIRO*. 2022, 189, 105–119. doi:10.36038/2307-3497-2022-189-105-119 (in Russian).
16. *Suzuki K.*, *Kanari S.* Tidal simulation of the Sea of Okhotsk. *Kaiyo Kagaku*. 1986, 18, 455–463 (in Japanese).
17. *Kowalik Z.*, *Polyakov I.* Tides in the Sea of Okhotsk. *Journal of Physical Oceanography*. 1998, 28(7), 1389–1409. doi:10.1029/93jc01363
18. *Moroz V.V.*, *Bogdanov K.T.*, *Rostov V.I.*, *Rostov I.D.* Electronic Atlas of tides of the marginal seas of the Northern Pacific. *Vestnik DVO RAN*. 2010, 1, 102–106 (in Russian).
19. *Nekrasov A.V.*, *Romanenkov D.A.* Impact of tidal power dams upon tides and environmental conditions in the Sea of Okhotsk. *Continental Shelf Research*. 2010, 30(6), 538–552. doi:10.1016/j.csr.2009.06.005
20. *Nakamura T.*, *Awaji T.*, *Hatayama T.*, *Kazunori A.* Tidal exchange through Kuril Straits. *Journal of Physical Oceanography*. 2000, 30, 1622–1644. doi:10.1175/1520–0485(2000)030<1622: TETTKS>2.0.CO;2
21. *Nakamura T.*, *Matthews J.P.*, *Awaji T.*, *Mitsudera H.* Submesoscale eddies near the Kuril Straits: Asymmetric generation of clockwise and counterclockwise eddies by barotropic tidal flow. *Journal of Geophysical Research. Oceans*. 2012, 117(C12). doi:10.1029/2011JC007754
22. *Tanaka Y.*, *Hibiya T.*, *Niwa Y.*, *Iwamae N.* Numerical study of K1 internal tides in the Kuril Straits. *Journal of Geophysical Research*. 2010, 115(C9). doi:10.1029/2009jc005903
23. *Zaron E.D.* Topographic and frictional controls on tides in the Sea of Okhotsk. *Ocean Modelling*. 2017, 117, 1–11. doi:10.1016/j.ocemod.2017.06.011
24. *Shu H.W.*, *Mitsudera H.*, *Yamazaki K.* et al. Tidally modified western boundary current drives interbasin exchange between the Sea of Okhotsk and the North Pacific. *Scientific Reports*. 2021, 11(12037). doi:10.1038/s41598-021-91412-y
25. *Lyubitsky Yu.V.* On assessing the quality of forecasts of total tidal sea levels. *Anniversary issue «FERHRI-65 years»*. *Vladivostok*, *Dalnauka*, 2015, 52–62.
26. *Rodionov A.A.*, *Androsov A.A.*, *Fofonova V.V.*, *Kuznetsov I.S.*, *Voltzinger N.E.* Modeling the tidal dynamics of the northern straits of the Kuril Ridge. *Fundamental and Applied Hydrophysics*. 2021, 14(3), 20–34. doi:10.7868/S2073667321030023 (in Russian).
27. *Efimov V.V.*, *Kulikov E.A.*, *Rabinovich A.B.*, *Fain I.V.* Ocean Boundary Waves. *Leningrad*, *Gidrometeoizdat*, 1985. 280 p. (in Russian).
28. *Shevchenko G.V., Romanov A.A.* Determination of diurnal shelf waves parameters in the area of north Kuril Islands from the satellite altimetry data. *Issledovanie Zemli iz Kosmosa*. 2008, 3, 76–87 (in Russian).
29. Tide tables. Harmonic constants for tide prediction. *Leningrad. Hydrographic Department of the Navy of USSR*. 1948. V. 2. 295 p. (in Russian).

30. Tide tables. Waters of the Asian Part of USSR and adjacent foreign regions. *Leningrad*, *Gidrometeoizdat*, 1960. 192 p. (in Russian).
31. Admiralty tide tables. Vol.41998. / NP 204. Pacific Ocean (Including tidal stream tables). *Taunton*, *Somerset*, *United Kingdom Hydrographic Office*, 1998. NP204.
32. National Data Buoy Center (NDBC). Current online. 2023. URL: https://www.ndbc.noaa.gov/station_page.php?station=21419; https://www.ndbc.noaa.gov/station_page.php?station=21416 (Accessed: 20.06.2023).
33. WXTIDE32. Windows tide and current prediction program. URL: http://www.wxtide32.com/ (Accessed: 20.06.2023).
34. *Androsov A.*, *Fofonova V.*, *Kuznetsov I.* et al. FESOM–C v.2: coastal dynamics on hybrid unstructured meshes. *Geoscientific Model Development*. 2019, 12, 1009–1028. doi:10.5194/gmd-12-1009–2019
35. *Zinchenko V.A.*, *Romanenkov D.A.*, *Androsov A.A.*, *Zinchenko V.A.*, *Romanenkov D.A.*, *Androsov A.A.* Comparison of the computational efficiency of the FESOM-c model for calculating coastal barotropic hydrodynamics using different unstructured meshes. *Processes in GeoMedia*. 2018, 3(17), 227–228 (in Russian).
36. *Kuznetsov I.*, *Androsov A.*, *Fofonova V.* et al. Evaluation and Application of Newly Designed Finite Volume Coastal Model FESOM–C, Effect of Variable Resolution in the Southeastern North Sea. *Water*. 2020, 12(5), 1412. doi:10.3390/w12051412
37. *Fofonova V.*, *Androsov A.*, *Sander L.* et al. Non-linear aspects of the tidal dynamics in the Sylt-Rømø Bight, south-eastern North Sea. *Ocean Science*. 2019, 15, 1761–1782. doi:10.5194/os-15-1761–2019
38. *Fofonova V.*, *Kärnä T.*, *Klingbeil K.* et al. Plume spreading test case for coastal ocean models. *Geoscientific Model Development*. 2021, 14(11), 6945–6975. doi:10.5194/gmd-14-6945–2021
39. *Geuzaine C.*, *Remacle J.-F.* Gmsh: a three-dimensional finite element mesh generator with built-in pre- and post-processing facilities. *International Journal for Numerical Methods in Engineering*. 2009, 79(11), 1309–1331. doi:10.1002/nme.2579
40. *Holt J.*, *Hyder P.*, *Ashworth M.* et al. Prospects for improving the representation of coastal and shelf seas in global ocean models. *Geoscientific Model Development*. 2017, 10, 499–523. doi:10.5194/gmd-10-499–2017
41. NOAA National Centers for Environmental Information. 2022: ETOPO 2022 15 Arc-Second Global Relief Model. NOAA National Centers for Environmental Information. doi:10.25921/fd45-gt74 (Accessed: 27.06.2023).
42. *Duvanin A.I.* Sea Tides. *Leningrad*, *Gidrometeoizdat*. 1960. 390 p. (in Russian).
43. Hydrometeorology and Hydrochemistry of the Seas. Vol. 9. The Okhotsk Sea. Part. 1. Hydrometeorological conditions. *St. Petersburg, Gidrometeoizdat*. 2003. 398 p. (in Russian).
44. *Shevchenko G.V.*, *Rabinovich A.B.*, *Thomson R.E.* Sea-ice drift on the Northeastern Shelf of Sakhalin Island. *Journal of Physical Oceanography*. 2004, 34(11), 2470–2491. doi:10.1175/JPO2632.1

Литература

1. *Stammer D.*, *Ray R.D.*, *Andersen O.B.* et al. Accuracy assessment of global barotropic ocean tide models // Reviews of Geophysics. 2014. Vol. 52. P. 243–282. doi:10.1002/2014RG000450
2. *Cipollini P., Benveniste J.*, *Birol F.* et al. Satellite altimetry in coastal regions. In: Satellite altimetry over oceans and land surfaces / Eds. Stammer D., Cazenave A. CRC Press: Boca Raton, FL, USA, 2017. P. 343–380. doi:10.1201/9781315151779-11
3. *Ranji Z.*, *Hejazi K.*, *Soltanpour M.*, *Allahyar M.R.* Inter-comparison of recent tide models for the Persian Gulf and Oman Sea // Coastal Engineering Proceedings. 2016. 35, currents. 9. doi:10.9753/icce.v35.currents.9
4. *Fu Y.*, *Feng Y.*, *Zhou D.* et al. Accuracy assessment of global ocean tide models in the South China Sea using satellite altimeter and tide gauge data // Acta Oceanologia Sinica. 2020. Vol. 39. P. 1–10. doi:10.1007/s13131-020-1685-y
5. *Sun W.*, *Zhou X.*, *Zhou D.*, *Sun Y.* Advances and accuracy assessment of ocean tide models in the Antarctic Ocean // Frontiers in Earth Science. 2022. Vol.10. doi:10.3389/feart.2022.757821
6. *Khomsin D.*, *Pratomo G.*, *Rohmawati C.N.* Analysis of accuracy comparison tidal global (FES2014, TPXO9) and regional (BIG Prediction) models to the existing tides in Surabaya and surrounding waters // IOP Conference Series: Earth and Environmental Science. 2021. N 936. P. 012028. doi:10.1088/1755-1315/936/1/012028
7. *Hart-Davis M.G.*, *Dettmering D.*, *Sulzbach R.* et al. Regional Evaluation of Minor Tidal Constituents for Improved Estimation of Ocean Tides // Remote Sensing. 2021. Vol. 13, iss. 16, N 3310. doi:10.3390/rs13163310
8. *Lee J.-C., Lee D-H.* Accuracy assessment of recent global ocean tide models using tide gauge measurements from the East Sea of Korea // Journal of Coastal Research. 2023. Vol. 39, N 2. P. 354–359. doi:10.2112/JCOASTRES-D-22TM-00010.1
9. *de Azkue M.F.*, *D'Onofrio E.E.*, *Jacobs A.* Assessing the accuracy of ocean tide models by using variance of residuals of satellite sea level heights in the Patagonian shelf // Anales Del Instituto De La Patagonia. 2022. Vol. 50. doi:10.22352/AIP202250004
10. *Ahn J.E.*, *Ronan A.D.* Impact of discrepancies between global ocean tide models on tidal simulations in the Shinnecock Bay area // Journal of Waterway, Port, Coastal, and Ocean Engineering. 2019. Vol. 145, N 2. doi:10.1061/(ASCE)WW.1943–5460.0000500

11. *Saraceno M.*, *D'Onofrio E.E.*, *Fiore M.E.*, *Grismeyer W.H.* Tide model comparison over the Southwestern Atlantic Shelf // Continental Shelf Research. 2010. Vol. 30, N 17. P. 1865–1875. doi:10.1016/j.csr.2010.08.014
12. *Ray R.D.*, *Loomis B.D.*, *Luthcke S.B.*, *Rachlin K.E.* Tests of ocean-tide models by analysis of satellite-to-satellite range measurements: an update // Geophysical Journal International. 2019. Vol. 217. P. 1174–1178. doi:10.1093/gji/ggz062
13. *Egbert G.D.*, *Erofeeva S.Y.* Efficient inverse modeling of barotropic ocean tides // Journal of Atmospheric and Oceanic Technology. 2002. Vol. 19, N 2. P. 183–204. doi:10.1175/1520-0426(2002)019<0183: EIMOBO>2.0.CO;2
14. *Lyard F.*, *Allain D.*, *Cancet M.*, *Carrère L.*, *Picot N.* FES2014 global ocean tide atlas: design and performance // Ocean Science, European Geosciences Union. 2021. Vol. 17. P. 615–649. doi:10.5194/os-17-615-2021
15. *Варкентин А.И.*, *Саушкина Д.Я.* О некоторых вопросах воспроизводства минтая в тихоокеанских водах, прилегающих к Камчатке и северным Курильским островам в 2013–2022 гг. // Труды ВНИРО. 2022. Vol. 189. P. 105–119. doi:10.36038/2307-3497-2022-189-105-119
16. *Suzuki K.*, *Kanari S.* Tidal simulation of the Sea of Okhotsk // Kaiyo Kagaku. 1986, Vol. 18 P. 455–463. (in Japanese)
17. *Kowalik Z., Polyakov I.* Tides in the Sea of Okhotsk // Journal of Physical Oceanography 1998. Vol. 28, N 7. P. 1389–1409. doi:10.1029/93jc01363
18. *Мороз В.В.*, *Богданов К.Т.*, *Ростов В.И.*, *Ростов И.Д.* Электронный атлас приливов окраинных морей северной Пацифики // Вестник ДВО РАН. 2010. № 1. С. 102–106.
19. *Nekrasov A.V.*, *Romanenkov D.A.* Impact of tidal power dams upon tides and environmental conditions in the Sea of Okhotsk // Continental Shelf Research. 2010. Vol. 30, N 6. P. 538–552. doi:10.1016/j.csr.2009.06.005
20. *Nakamura T.*, *Awaji T.*, *Hatayama T.*, *Kazunori A.* Tidal exchange through Kuril Straits // Journal of Physical Oceanography. 2000. Vol. 30. P. 1622–1644. doi:10.1175/1520-0485(2000)030<1622: TETTKS>2.0.CO;2
21. *Nakamura T.*, *Matthews J.P.*, *Awaji T.*, *Mitsudera H.* Submesoscale eddies near the Kuril Straits: Asymmetric generation of clockwise and counterclockwise eddies by barotropic tidal flow // Journal of Geophysical Research. Oceans. 2012. Vol. 117, N C12. doi:10.1029/2011JC007754
22. *Tanaka Y.*, *Hibiya T.*, *Niwa Y.*, *Iwamae N.* Numerical study of K1 internal tides in the Kuril Straits // Journal of Geophysical Research. 2010. Vol. 115, N C9. doi:10.1029/2009jc005903
23. *Zaron E.D.* Topographic and frictional controls on tides in the Sea of Okhotsk // Ocean Modelling. 2017. Vol. 117. P. 1–11. doi:10.1016/j.ocemod.2017.06.011
24. *Shu H.W.*, *Mitsudera H.*, *Yamazaki K.* et al. Tidally modified western boundary current drives interbasin exchange between the Sea of Okhotsk and the North Pacific // Scientific Reports. 2021. Vol. 11, N 12037. doi:10.1038/s41598-021-91412-y
25. *Любицкий Ю.В.* Об оценке качества прогнозов суммарных уровней приливного моря // Юбилейный выпуск «ДВНИГМИ-65 лет». Владивосток: Дальнаука, 2015. С. 52–62.
26. *Родионов А.А.*, *Андросов А.А.*, *Фофонова В.В.*, *Кузнецов И.С.*, *Вольцингер Н.Е.* Моделирование приливной динамики северных проливов Курильской гряды // Фундаментальная и прикладная гидрофизика. 2021. Т. 14, № 3. С. 20–34. doi:10.7868/S2073667321030023
27. *Ефимов В.В.*, *Куликов Е.А.*, *Рабинович А.Б.*, *Файн И.В.* Волны в пограничных областях океана. Л.: Гидрометеоиздат, 1985. 280 с.
28. *Шевченко Г.В.*, *Романов А.А.* Определение параметров суточных приливных шельфовых волн в районе Северных Курильских островов по данным спутниковой альтиметрии // Исследование Земли из космоса. 2008. № 3. С. 76–87.
29. Таблицы приливов. Гармонические постоянные для предвычисления приливов. Л.: Изд. Гидрографического управления ВМФ СССР. 1948. Т. 2. 295 с.
30. Таблицы приливов. Воды Азиатской части СССР и прилегающих зарубежных районов. Л.: Гидрометеоиздат, 1960. 192 с.
31. Admiralty tide tables. Vol.41998. / NP 204. Pacific Ocean (Including tidal stream tables). Taunton, Somerset: United Kingdom Hydrographic Office. 1998. NP204.
32. National Data Buoy Center (NDBC). Current online. 2023. URL: https://www.ndbc.noaa.gov/station_page.php?station=21419; https://www.ndbc.noaa.gov/station_page.php?station=21416 (дата обращения: 20.06.2023).
33. WXTIDE32. Windows tide and current prediction program. URL: http://www.wxtide32.com/ (дата обращения: 20.06.2023).
34. *Androsov A.*, *Fofonova V.*, *Kuznetsov I.* et al. FESOM–C v.2: coastal dynamics on hybrid unstructured meshes // Geoscientific Model Development. 2019. Vol. 12. P. 1009–1028. doi:10.5194/gmd-12–1009–2019
35. *Зинченко В.А.*, *Романенков Д.А.*, *Андросов А.А.* Сравнение вычислительной эффективности модели FESOM-c для расчета прибрежной баротропной гидродинамики при использовании различных неструктурированных сеток // Процессы в геосредах. 2018. № 3 (17). С. 227–228.
36. *Kuznetsov I.*, *Androsov A.*, *Fofonova V.* et al. Evaluation and Application of Newly Designed Finite Volume Coastal Model FESOM–C, Effect of Variable Resolution in the Southeastern North Sea // Water. 2020. Vol. 12, N 5. P. 1412. doi:10.3390/w12051412

37. *Fofonova V.*, *Androsov A.*, *Sander L.* et al. Non-linear aspects of the tidal dynamics in the Sylt-Rømø Bight, south-eastern North Sea // Ocean Science. 2019. Vol. 15. P. 1761–1782. doi:10.5194/os-15-1761–2019
38. *Fofonova V.*, *Kärn*ä *T.*, *Klingbeil K.* et al. Plume spreading test case for coastal ocean models // Geoscientific Model Development. 2021. Vol. 14, N 11. P. 6945–6975. doi:10.5194/gmd-14-6945–2021
39. *Geuzaine C.*, *Remacle J.-F.* Gmsh: a three-dimensional finite element mesh generator with built-in pre- and post-processing facilities // International Journal for Numerical Methods in Engineering. 2009. Vol. 79, N 11. P. 1309–1331. doi:10.1002/nme.2579
40. *Holt J.*, *Hyder P.*, *Ashworth M.* et al. Prospects for improving the representation of coastal and shelf seas in global ocean models // Geoscientific Model Development. 2017. Vol. 10. P. 499–523. doi:10.5194/gmd-10-499–2017
41. NOAA National Centers for Environmental Information. 2022: ETOPO 2022 15 Arc-Second Global Relief Model. NOAA National Centers for Environmental Information. doi: 10.25921/fd45-gt74 (дата обращения: 27.06.2023).
42. *Дуванин А.И.* Приливы в море. Л.: Гидрометеоиздат, 1960. 390 с.
43. Гидрометеорология и гидрохимия морей. Т. IX. Охотское море. Вып. 1. Гидрометеорологические условия / Под ред. Б.Х. Глуховского, Н.П. Гоптарева, Ф.С. Терзиева. СПб.: Гидрометеоиздат, 2003. 398 с.
44. *Shevchenko G.V.*, *Rabinovich A.B.*, *Thomson R.E.* Sea-ice drift on the Northeastern Shelf of Sakhalin Island // Journal of Physical Oceanography. 2004. Vol. 34, N 11. P. 2470–2491. doi:10.1175/JPO2632.1

About the Authors

ROMANENKOV, Dmitry A, Cand. Sc. (Geogr.), РИНЦ AuthorID: 61515, ORCID ID: 0009-0005-0374-486X, Scopus AuthorID: 6506855768, WoS ResearcherID: U-8280-2017, dmromanenkov@yandex.ru

SOFINA, Ekaterina V., Cand. Sc. (Phys.-Math.), РИНЦ AuthorID: 169097, ORCID ID: 0000-0001-9206-8253, Scopus AuthorID: 23111468200, WoS ResearcherID: E-3920–2014, sofjina_k@mail.ru

RODIKOVA, Aleksandra Ye., rodikovaa99@gmail.com